

Joint learning of Gaussian graphical models in heterogeneous dependencies of high-dimensional transcriptomic data

Dung Ngoc Nguyen `NGOCDUNG.NGUYEN@CSIRO.AU` and **Zitong Li** `ZITONG.LI@CSIRO.AU`
CSIRO Agriculture and Food, Canberra, ACT, Australia.

Editors: Vu Nguyen and Hsuan-Tien Lin

Abstract

In biology, constructing gene co-expression networks presents a significant research challenge, largely due to the high dimensionality of the data and the heterogeneity of the samples. Furthermore, observations from two or more groups sharing the same biological variables require the comparison of gene co-expression patterns with some commonalities between the groups. In this context, we propose a mixture of Gaussian graphical models for paired data to estimate heterogeneous dependencies and uncover sub-population networks within complex biological datasets, incorporating sparsity and symmetry constraints between two groups of dependent variables. We develop an efficient generalized expectation-maximization (EM) algorithm for penalized maximum likelihood estimation with the fusion of a graphical lasso penalty. As a result, our simulation studies highlight the numerical performance of the proposed method, demonstrating its superior model fitting compared to the classical graphical lasso approach. We further demonstrate the practical application of our approach by estimating gene networks on a high-dimensional ecological transcriptomics data set of the nine-spined stickleback. Our new approach identified similarities and differences between groups of genes from the brain and liver tissues of samples collected from two habitats. These results show the efficiency of our approach to the identification of complicated interactions from high-dimensional and heterogeneous gene expression data.

Keywords: Mixture Gaussian graphical models; Paired data; Penalized maximum likelihood; EM algorithm; Unsupervised machine learning; Bioinformatics.

1. Introduction

With recent advances in the development of cost-effective high-throughput RNA sequencing technology (Stark et al. (2019)), gene co-expression network analysis (D’haeseleer et al. (2000); López-Kleine et al. (2013); Rao and Dixon (2019)) has become increasingly popular for studying the complex interactions between genes, proteins, and regulatory elements, identifying functionally related groups of genes and how they contribute to the expression of desirable traits, and understanding the biological factors underlying phenotypic diversity. The Gaussian graphical model (GGM), introduced by Dempster (1972), is one of the most commonly and widely applied tools for analyzing biological networks. This is a family of multivariate Gaussian models with restriction of the conditional independence of selected pairs of variables, given the others, in terms of an undirected graph. Each vertex in the graph represents a variable, and the absence of an edge implies that the corresponding entry in the concentration matrix, i.e. the inverse of the covariance matrix, is equal to zero, see Lauritzen (1996). Inference from these models, when applied to large-scale molecular biology experiments, enables us to account for the correlation of marker effects in predicting

41 gene functions, phenotypes, and molecular regulation patterns. See [Ursem et al. \(2008\)](#),
 42 [Valcarcel et al. \(2011\)](#), [Ma et al. \(2007\)](#), [Chang and McGeachie \(2011\)](#), [Kurtz et al. \(2015\)](#),
 43 [Zheng et al. \(2020\)](#) and references therein.

44 In biological applications, it is common for observed data to originate from various
 45 sources and exhibit heterogeneous dependencies across the entire population. Addition-
 46 ally, gene expression data are often collected from different treatments or across different
 47 tissues, cells, or phenotypes, generating interest in comparing gene co-expression patterns
 48 under distinct experimental conditions or between groups. In this paper, we focus on the
 49 joint learning of a mixture of Gaussian graphical models for paired data in heterogeneous
 50 populations, with an emphasis on high-dimensional scenarios. Different sub-populations or
 51 classes are modeled by distinct networks. For every sub-population, we assume the presence
 52 of exactly two dependent groups of homologous variables, i.e. representing two experimental
 53 conditions, with the association structure of each group captured by a corresponding sub-
 54 network. The two sub-networks within each sub-population are interconnected, with edges
 55 linking vertices both within and between the sub-networks. Similarities between groups are
 56 represented using graph coloring ([Højsgaard and Lauritzen \(2008\)](#)), where vertex coloring
 57 represents equality constraints on the diagonal entries of the concentration matrix and edge
 58 coloring represents equality constraints on the off-diagonal entries. We refer to this class of
 59 models as *a mixture of graphical models for paired data with restrictions on concentrations*
 60 or *mixture of pdRCON models* for short.

61 2. Related works and Contribution

62 Heterogeneity is a common characteristic in biological studies, where samples are often
 63 measured at different locations or originate from distinct populations or families. In the
 64 relevant literature, the mixture of graphical models has proven useful for uncovering genomic
 65 variations in high-throughput sequencing data that cannot be adequately captured with a
 66 single distribution ([Liang and Jia \(2023\)](#)). Recent studies employing this type of graphical
 67 model for analyzing omics data in quantitative genomics include [Blein-Nicolas et al. \(2024\)](#),
 68 [Danaher et al. \(2014\)](#). The former study extended the novel block-diagonal covariance for
 69 locally linear Gaussian mapping and applied this model to predict drought-related traits
 70 from protein abundance in maize. Whereas the latter introduced the joint graphical lasso
 71 to simultaneously construct multiple graphical models for distinct but related conditions,
 72 analyzing lung cancer microarray data. For further application, see [Lotsi and Wit \(2016\)](#),
 73 [Lee and Xue \(2018\)](#), [Lartigue et al. \(2021\)](#), and the references therein.

74 Moreover, comparing the distribution of a set of variables between two experimental
 75 conditions or groups is a key focus in numerous applications. When the association struc-
 76 ture represented by a GGM is of interest, analyzing paired data can be framed as the joint
 77 learning of a graph structure of each group, with particular attention to the cross-sectional
 78 association structure between the two graphs. Joint learning of dependent GGMs is com-
 79 monly applied in genomics to compare co-expression patterns between healthy and cancer
 80 tissues, as reflected in the transcriptional networks, see [Hardcastle and Kelly \(2013\)](#); [Dana-
 81 her et al. \(2014\)](#); [Aran et al. \(2017\)](#). Another example involves the comparison of brain
 82 networks derived from fMRI data, which often exhibit naturally symmetrical structures
 83 between the two hemispheres. In this context, [Roverato and Nguyen \(2022, 2024\)](#) explored

84 the search space of pdRCON models using an efficient backward elimination procedure to
85 better understand the structure of this model class. While this approach offered a fast
86 model selection method, model identification remains challenging due to the high dimen-
87 sionality and complexity of the model space. Alternatively, penalized maximum likelihood
88 methods have been proposed to address high dimensionality by avoiding explicit exploration
89 of the model space, potentially yielding solutions closer to the global optimum compared to
90 the backward selection. Recent works of [Ranciati et al. \(2021\)](#) and [Ranciati and Roverato \(2023\)](#)
91 introduced the graphical lasso for paired data (pdglasso) which extends the sym-
92 metric graphical lasso method for the class of GGMs to analyze paired data. These studies
93 also developed an alternating directions method of multiplier (ADMM) algorithm to solve
94 the pdglasso optimization tasks.

95 We develop a novel penalized expectation-maximization (EM) algorithm that simulta-
96 neously clusters individuals and infers the graph structure by adapting the original pdglasso
97 methods, initially introduced by [Ranciati et al. \(2021\)](#); [Ranciati and Roverato \(2023\)](#), to
98 each sub-population. Specifically, we use the graphical lasso to induce sparsity within
99 groups and the fused graphical lasso to enforce graph symmetries between groups of vari-
100 ables. Regularization parameters are selected based on the asymptotic consistency of the
101 extended Bayesian information criterion (eBIC) ([Foygel and Drton \(2010\)](#)), adapted for
102 GGMs in scenarios where both the sample size and the number of variables are compara-
103 ble. The efficiency of our approach is demonstrated by constructing gene networks using
104 both synthetic data sets and real-world ecological transcriptome datasets from nine-spined
105 sticklebacks, including a comparison of our method with the classical graphical lasso on
106 synthetic data. Our method provides a robust tool for reconstructing gene co-expression
107 networks, exploring similar expression patterns within and between condition groups, and
108 clustering individuals based on shared biological characteristics. The potential applications
109 of this approach extend beyond the gene co-expression network, including its use in con-
110 structing other high-dimensional biological networks such as microbial interaction networks
111 ([Faust \(2021\)](#)), brain connectivity networks ([Bullmore and Bassett \(2011\)](#)), as well as in
112 disease-gene association prediction ([Miller and Bishop \(2021\)](#)).

113 The rest of the paper is organized as follows. Section 3 provides an overview of the
114 mixture of GGMs for addressing heterogeneity, along with penalized maximum likelihood
115 estimations using graphical lasso penalty. In the same section, we introduce the family of
116 mixtures of RCON models for paired data, incorporating a fused lasso penalty that enables
117 simultaneously learning of both the network structure and similarity between two groups
118 of variables. Section 4 describes a penalized EM algorithm for model estimation, with its
119 application to both synthetic and real-world data presented in Section 5. Finally, Section
120 6 offers a brief discussion and concluding remarks. Technical details for EM algorithm and
121 additional results from the numerical experiments are provided in the Supplementary.

122 3. The models

123 This section focuses on classes of Gaussian mixture graphical models, particularly those
124 designed to address the paired data problems. It also covers the fusion of the graphical
125 lasso applied to each sub-population in heterogeneous and high-dimensional datasets.

126 **3.1. Mixture of Gaussian graphical models**

127 Let $\mathbf{Y} = (Y_1, \dots, Y_P)$ be a vector of continuous random variables indexed by $V = \{1, \dots, P\}$
 128 with the observation $\mathbf{y} \in \mathbb{R}^P$. In heterogeneous populations, observations are assumed to
 129 originate from one of K different network models. We define $\mathbf{Z} = (Z_1, \dots, Z_K)$ as the vector
 130 of binary latent variables, where $Z_k = 1$ indicates that the observation \mathbf{y} belongs to the
 131 k -th class. We model each class separately by assuming a Gaussian graphical model (GGM)
 132 for \mathbf{Y} , where $(\mathbf{Y} \mid Z_k = 1) \sim \mathcal{N}(0, \Theta_k^{-1})$, with the concentration matrix Θ_k corresponding
 133 to the undirected graph G_k . Specifically, each missing edge in the graph implies that the
 134 corresponding entry of the concentration matrix is zero. In GGMs, the zero pattern of
 135 the concentration matrix reflects the conditional independence between two corresponding
 136 variables in the joint distribution. Our interest lies in the structure of Θ . Therefore, without
 137 loss of generality, we assume throughout the paper that the random variables \mathbf{Y} have zero
 138 means. The GGM of $\mathbf{Y} \mid \mathbf{Z}$ with respect to G_k can be expressed as

$$p(\mathbf{y} \mid Z_k = 1, \Theta_k) = (2\pi)^{-P/2} \det(\Theta_k)^{1/2} \exp\left(-\frac{\mathbf{y}^T \Theta_k \mathbf{y}}{2}\right), \quad (1)$$

139 where Θ_k is a positive-definite concentration matrix restricted on graph G_k . By marginal-
 140 izing equations (1) according to the latent variable \mathbf{Z} , the density of \mathbf{Y} is then specified as
 141 the weighted multivariate Gaussian graphical models, which is

$$p(\mathbf{y} \mid \mathbf{w}, \Theta) = \sum_{k=1}^K w_k p(\mathbf{y} \mid Z_k = 1, \Theta_k) \quad (2)$$

142 with the parameter vectors $\mathbf{w} = (w_1, \dots, w_K)$ and $\Theta = (\Theta_1, \dots, \Theta_K)$, where for $k =$
 143 $1, \dots, K$, the probability $\mathbb{P}(Z_k = 1) = w_k$ represents the mixture proportion, subject to
 144 $\sum_{k=1}^K w_k = 1$, and $p(\mathbf{y} \mid Z_k = 1, \Theta_k)$ refers to a GGM defined in (1) with respect to G_k .

145 For a sample of independent and identically distributed observations $\mathbf{y}_1, \dots, \mathbf{y}_N$ and the
 146 allocation values $\mathbf{Z}_n = (Z_{n1}, \dots, Z_{nK})$ associated with the observation \mathbf{y}_n , the maximum
 147 likelihood estimations (MLE) of (\mathbf{w}, Θ) are the values that maximize the log-likelihood
 148 function

$$l(\mathbf{w}, \Theta) = \sum_{n=1}^N \log \left\{ \sum_{k=1}^K w_k p(\mathbf{y}_n \mid Z_{nk} = 1, \Theta_k) \right\}. \quad (3)$$

149 To handle high-dimensional settings, which are particularly common in genomics, graph-
 150 ical lasso (glasso) (Yuan and Lin (2007), Friedman et al. (2008)) has been widely used to
 151 estimate precision matrices by incorporating a lasso penalty term into the likelihood func-
 152 tion, producing sparse solutions. Specifically, in Gaussian mixture graphical models, sparse
 153 estimators of Θ can be obtained by minimising the penalized log-likelihood function

$$l_{\lambda_1, \dots, \lambda_K}(\mathbf{w}, \Theta) = -l(\mathbf{w}, \Theta) + \sum_{k=1}^K \lambda_k \|\Theta_k\|_1, \quad (4)$$

154 where $l(\cdot)$ is the log-likelihood function defined in (3), and $\|\cdot\|_1$ denotes the l_1 -norm, which
 155 is the sum of the absolute values of the matrix entries. Here, the regularization parameters

156 $\lambda_1, \dots, \lambda_K$ are non-negative and control the level of penalization for each sub-population.
 157 For every class k , as λ_k increase, the off-diagonal entries of the concentration matrix are
 158 shrunk towards zero. This allows the graphical lasso to perform the estimation and model
 159 selection simultaneously within the GGM framework. For various applications of the glasso
 160 and its variant in heterogeneous data, see [Zhou et al. \(2009\)](#); [Lotsi and Wit \(2016\)](#); [Lartigue](#)
 161 [et al. \(2021\)](#).

162 3.2. Mixture of RCON models for paired data

163 **Paired data.** In a paired data problem, the variables on every statistical unit are mea-
 164 sured twice from two different conditions, e.g. across different tissues or treatments. There-
 165 fore, the random vector \mathbf{Y} is partitioned into two sets of homologous variables $\mathbf{Y} =$
 166 $(\mathbf{Y}_L, \mathbf{Y}_R)$ so that every variable $Y_i \in \mathbf{Y}_L$ corresponds to a homologous variable $Y_j \in \mathbf{Y}_R$.
 167 Accordingly, the concentration matrix Θ is naturally divided into blocks such that

$$\Theta = \begin{pmatrix} \Theta^{LL} & \Theta^{LR} \\ \Theta^{RL} & \Theta^{RR} \end{pmatrix}.$$

168 The interest is in explicitly studying symmetries between and across the two sub-networks
 169 in the form of identities of concentrations in Θ^{LL} with the corresponding concentration in
 170 Θ^{RR} and identities of concentrations in Θ^{LR} with the corresponding concentrations in Θ^{RL} .
 171 Symmetries can be presented by graph colorings.

172 **RCON models for paired data (pdRCON).** [Roverato and Nguyen \(2022\)](#) approached
 173 the paired data problems by introducing the class of colored graphs for paired data (pdCGs)
 174 denoted by $\mathcal{G} = (\mathcal{V}, \mathcal{E})$. Each vertex of the graph presents a random variable and the
 175 associated graph can be split into two sub-networks corresponding to the vertex sets, called
 176 $L = \{1, \dots, Q\}$ and $R = \{1', \dots, Q'\}$, with $Q = P/2$ and $i' = i + Q$ for $i \in L$, so that
 177 $V = L \cup R$ and $L \cap R = \emptyset$. The vertex coloring $\mathcal{V} = \{V_1, \dots, V_v\}$ is a partition of V with
 178 specific types of color classes that is either twin-pairing $\{i, i'\}$ or atomic $\{i\}$, and the edge
 179 coloring $\mathcal{E} = \{E_1, \dots, E_e\}$ is a partition of the edge set E into edge color classes that is
 180 twin-pairing $\{(i, j), (i', j')\}$ between groups or $\{(i, j'), (i', j)\}$ across groups, or atomic class
 181 with single edge element. In the graphical representation, if two homologous vertices or
 182 edges belong to a twin-pairing class, they are depicted in the same color. For vertices and
 183 edges of the atomic classes, they are all depicted in black.

184 RCON models for paired data (pdRCONs) are GGMS with additional equality con-
 185 straints of the concentrations restricted by a pdCG \mathcal{G} . In particular, the vertex class $\{i, i'\}$
 186 implies the equality of diagonal entries $\theta_{ii} = \theta_{i'i'}$ and the edge classes $\{(i, j), (i', j')\}$ and
 187 $\{(i, j'), (i', j)\}$ imply the equality of off-diagonal entries $\theta_{ij} = \theta_{i'j'}$ and $\theta_{ij'} = \theta_{i'j}$, respec-
 188 tively. For vertices and edges belonging to the atomic color classes, there are no equality re-
 189 strictions of the associated parameters in the model. In this way, equality constraints reveal
 190 symmetries concerning both the structure of the network and the values of the parameters
 191 associated with vertices and edges and also have the practical advantage of reducing the
 192 number of parameters, see [Roverato and Nguyen \(2022, 2024\)](#) for more information.

193 **Mixture of pdRCON models.** With K classes in the heterogeneous data, we denote
 194 $\Theta_{\mathcal{G}} = (\Theta_{\mathcal{G}_1}, \dots, \Theta_{\mathcal{G}_K})$ the concentration matrices restricted on pdCGs $\mathcal{G} = (\mathcal{G}_1, \dots, \mathcal{G}_K)$.

195 The density of \mathbf{Y} is then specified as a mixture of weighted pdRCON models, which is

$$p(\mathbf{y} \mid \mathbf{w}, \Theta_{\mathcal{G}}) = \sum_{k=1}^K w_k p(\mathbf{y} \mid Z_k = 1, \Theta_{\mathcal{G}_k}). \quad (5)$$

196 To learn both sparsity in the graph structures and similarities between two groups in the
 197 heterogeneous data, we apply the *fused lasso* to every sub-population model. The estimators
 198 of $(\mathbf{w}, \Theta_{\mathcal{G}})$ are then obtained by

$$(\hat{\mathbf{w}}, \hat{\Theta}_{\lambda_1, \lambda_2}) = \underset{\mathbf{w}, \Theta_{\mathcal{G}}}{\operatorname{argmin}} - \frac{1}{N} \sum_{n=1}^N \log \left\{ \sum_{k=1}^K w_k p(\mathbf{y}_n \mid Z_{nk} = 1, \Theta_{\mathcal{G}_k}) \right\} + \operatorname{pen}_{\lambda_1, \lambda_2}(\Theta_{\mathcal{G}}) \quad (6)$$

199 where $p(\mathbf{y}_n \mid Z_{nk} = 1, \Theta_{\mathcal{G}_k})$ specified in (1) is a GGM with respect to pdCG \mathcal{G}_k and the
 200 penalty function

$$\operatorname{pen}_{\lambda_1, \lambda_2}(\Theta_{\mathcal{G}}) = \sum_{k=1}^K \lambda_k^{[1]} \|\Theta_{\mathcal{G}_k}\|_1 + \sum_{k=1}^K \lambda_k^{[2]} \|\Theta_{\mathcal{G}_k}^{LL} - \Theta_{\mathcal{G}_k}^{RR}\|_1 + \sum_{k=1}^K \lambda_k^{[2]} \|\Theta_{\mathcal{G}_k}^{LR} - \Theta_{\mathcal{G}_k}^{RL}\|_1, \quad (7)$$

201 with $\lambda_1 = (\lambda_1^{[1]}, \dots, \lambda_K^{[1]})$, $\lambda_2 = (\lambda_1^{[2]}, \dots, \lambda_K^{[2]})$ denoting the non-negative regularization
 202 parameter vectors. The first term of (7) encourages sparsity in the graph structure to each
 203 class k controlled by $\lambda_k^{[1]}$, and the last two terms encourage the identities of $\hat{\Theta}_k^{LL}$ and $\hat{\Theta}_k^{RR}$
 204 between groups and the identities of $\hat{\Theta}_k^{LR}$ and $\hat{\Theta}_k^{RL}$ across groups controlled by $\lambda_k^{[2]}$. Here,
 205 we do not introduce any penalty to \mathbf{w} given the fact that its dimension is unlikely to be
 206 high in most of the biological applications. Because (6) is a non-convex problem and it is
 207 difficult to obtain MLE in a direct way, we develop a penalized expectation-maximization
 208 (EM) algorithm to find maximum likelihood estimates for models with latent variables.

209 4. Penalized EM algorithm for the mixture of pdRCON models

210 In fact, if we know the variable \mathbf{Z} we can simply derive the estimations through the samples
 211 of \mathbf{Y} such that $(\mathbf{Y} \mid Z_k = 1) \sim \mathcal{N}(0, \Theta_{\mathcal{G}_k}^{-1})$. Generally, \mathbf{Z} is unobserved, we thus use the
 212 posterior probability $p(\mathbf{Z} \mid \mathbf{Y})$ to approximate \mathbf{Z} . In this section, we describe a more abstract
 213 view of the penalized EM algorithm for the mixture of pdRCON models via complete data.
 214 A more detailed of the computational algorithm is given in Section S1 of the Supplementary.

215 4.1. Penalized complete log-likelihood function

216 For the complete data $\mathcal{D}_c = \{(\mathbf{y}_1, \mathbf{z}_1), \dots, (\mathbf{y}_N, \mathbf{z}_N)\}$, the complete log-likelihood of $(\mathbf{w}, \Theta_{\mathcal{G}})$
 217 can be computed as

$$l_{\lambda_1, \lambda_2}(\mathcal{D}_c \mid \mathbf{w}, \Theta_{\mathcal{G}}) = \sum_{n=1}^N \sum_{k=1}^K z_{nk} \left(\log w_k + \log p(\mathbf{y}_n \mid \Theta_{\mathcal{G}_k}) \right) - \operatorname{pen}_{\lambda_1, \lambda_2}(\Theta_{\mathcal{G}}),$$

218 where $\operatorname{pen}_{\lambda_1, \lambda_2}(\cdot)$ is the fused lasso penalty function defined in (7). In practice, we can-
 219 not derive the value of the (penalized) complete log-likelihood function due to unobserved

220 variables \mathbf{Z}_n , we consider the expectation of the (penalized) complete log-likelihood with
 221 respect to the posterior of the latent variables, which is

$$\mathbb{E}_{\mathbf{Z}|\mathbf{Y}}\left(l_{\lambda_1, \lambda_2}(\mathcal{D}_c | \mathbf{w}, \Theta_{\mathcal{G}})\right) = \sum_{n=1}^N \sum_{k=1}^K \tau_{nk} \left(\log w_k + \log p(\mathbf{y}_n | \Theta_{\mathcal{G}_k}) \right) - \text{pen}_{\lambda_1, \lambda_2}(\Theta_{\mathcal{G}}) \quad (8)$$

222 where τ_{nk} is denoted the conditional expectation of Z_{nk} given observations \mathbf{y}_n , which can
 223 be specified by using Bayes' theorem, for every $n \in \{1, \dots, N\}$, $k \in \{1, \dots, K\}$, as

$$\begin{aligned} \tau_{nk} &= \mathbb{E}_{\mathbf{Z}|\mathbf{Y}}(Z_{nk}) = \mathbb{P}(Z_{nk} = 1 | \mathbf{y}_n, \mathbf{w}, \Theta_{\mathcal{G}}) \\ &= \frac{p(\mathbf{y}_n, | Z_{nk} = 1, \Theta_{\mathcal{G}}, \mathbf{w}) \times \mathbb{P}(Z_{nk} = 1 | \mathbf{w})}{p(\mathbf{y}_n | \Theta_{\mathcal{G}}, \mathbf{w})} \\ &= \frac{w_k p(\mathbf{y}_n | \Theta_{\mathcal{G}_k})}{\sum_{l=1}^K w_l p(\mathbf{y}_n | \Theta_{\mathcal{G}_l})}. \end{aligned} \quad (9)$$

224 The quantity τ_{nk} is known as the posterior distribution of Z_{nk} given the observations and
 225 is used to find the MLE of the model parameters in the EM algorithm, which is described
 226 in the following section.

227 4.2. The algorithm

228 EM algorithm alternates between the expectation step (E-step), which computes the con-
 229 ditional expectation of the penalized complete log-likelihood with current values of param-
 230 eters, and the maximization step (M-step), which updates the parameters based on maxi-
 231 mizing the conditional expectation computed in E-step, until convergence, e.g., when there
 232 is no longer significant change in the variation of the parameter estimation. In particular,

233 **(E-step)** given the observed data $\mathbf{y}_1, \dots, \mathbf{y}_N$ with current values of parameters $(\mathbf{w}^{(t)}, \Theta_{\mathcal{G}}^{(t)})$
 234 at t -th iteration of the algorithm, the posterior distribution of the latent variables is given
 235 by $\tau_{nk}^{(t)} = p(Z_{nk} | \mathbf{y}_n, \mathbf{w}^{(t)}, \Theta_{\mathcal{G}}^{(t)})$ specified by (9).

236 **(M-step)** We use $\tau_{nk}^{(t)}$ to evaluate the conditional expectation of the penalized complete
 237 log-likelihood, which is defined by

$$O_{\text{pen}}\left((\mathbf{w}, \Theta_{\mathcal{G}}), (\mathbf{w}^{(t)}, \Theta_{\mathcal{G}}^{(t)})\right) = \sum_{n=1}^N \sum_{k=1}^K \tau_{nk}^{(t)} \left(\log w_k + \log p(\mathbf{y}_n | \Theta_{\mathcal{G}_k}) \right) - \text{pen}_{\lambda_1, \lambda_2}(\Theta_{\mathcal{G}}). \quad (10)$$

238 We observe that (10) can be decomposed into independent expressions as

$$O_{\text{pen}}\left((\mathbf{w}, \Theta_{\mathcal{G}}), (\mathbf{w}^{(t)}, \Theta_{\mathcal{G}}^{(t)})\right) = O(\mathbf{w}, \mathbf{w}^{(t)}) + O_{\text{pen}}(\Theta_{\mathcal{G}}, \Theta_{\mathcal{G}}^{(t)}),$$

239 where

$$\begin{aligned} O(\mathbf{w}, \mathbf{w}^{(t)}) &= \sum_{n=1}^N \sum_{k=1}^K \tau_{nk}^{(t)} \log w_k, \quad \text{and} \\ O_{\text{pen}}(\Theta_{\mathcal{G}}, \Theta_{\mathcal{G}}^{(t)}) &= \sum_{n=1}^N \sum_{k=1}^K \tau_{nk}^{(t)} \log p(\mathbf{y}_n | \Theta_{\mathcal{G}_k}) - \text{pen}_{\lambda_1, \lambda_2}(\Theta_{\mathcal{G}}). \end{aligned}$$

240 We update new parameters $(\mathbf{w}^{(t+1)}, \Theta_{\mathcal{G}}^{(t+1)})$ by separately maximizing the two independent
 241 components of (10) as follows:

242 1. **Update mixture proportion $\mathbf{w}^{(t+1)}$.** By applying the Lagrange multiplier method
 243 to constraint $\sum_{k=1}^K w_k = 1$, we obtain the new update of w_k as

$$\widehat{w}_k^{(t+1)} = N_k^{(t)} / N \quad \text{with } N_k^{(t)} = \sum_{n=1}^N \tau_{nk}^{(t)} \quad (11)$$

244 where $N_k^{(t)}$ is denoted as the effective number of observations assigned to class k .

245 2. **Update models' parameters $\Theta_{\mathcal{G}}$.** The second term of (10) can be written as

$$\begin{aligned} & O_{\text{pen}}(\Theta_{\mathcal{G}}, \Theta_{\mathcal{G}}^{(t)}) \\ &= \sum_{n=1}^N \sum_{k=1}^K \tau_{nk}^{(t)} \log p(\mathbf{y}_n | \Theta_{\mathcal{G}_k}) - \sum_{k=1}^K \lambda_k^{[1]} \|\Theta_{\mathcal{G}_k}\|_1 - \sum_{k=1}^K \lambda_k^{[2]} \left(\|\Theta_{\mathcal{G}_k}^{LL} - \Theta_{\mathcal{G}_k}^{RR}\|_1 + \|\Theta_{\mathcal{G}_k}^{LR} - \Theta_{\mathcal{G}_k}^{RL}\|_1 \right) \\ &= \frac{1}{2} \sum_{k=1}^K N_k^{(t)} \left[\log \det(\Theta_{\mathcal{G}_k}) - \text{tr}(S_k^{(t)} \Theta_{\mathcal{G}_k}) \right] \\ &\quad - \sum_{k=1}^K \lambda_k^{[1]} \|\Theta_{\mathcal{G}_k}\|_1 - \sum_{k=1}^K \lambda_k^{[2]} \left(\|\Theta_{\mathcal{G}_k}^{LL} - \Theta_{\mathcal{G}_k}^{RR}\|_1 + \|\Theta_{\mathcal{G}_k}^{LR} - \Theta_{\mathcal{G}_k}^{RL}\|_1 \right), \end{aligned} \quad (12)$$

246 where, for $k \in \{1, \dots, K\}$, $S_k^{(t)} = \sum_{n=1}^N \tau_{nk}^{(t)} \mathbf{y}_n^T \mathbf{y}_n / N_k^{(t)}$ is denoted as a weighted sample
 247 covariance matrix, and $\text{tr}(\cdot)$ is denoted the trace of a square matrix, i.e. the sum of
 248 elements on the main diagonal entries. As shown in (12), performing the update for
 249 the Gaussian networks' parameters corresponds to solving K separated fused lasso
 250 problems using the alternating direction method of multiplier (ADMM) algorithm
 251 proposed by [Boyd et al. \(2011\)](#). In particular, for every $k \in \{1, \dots, K\}$,

$$\begin{aligned} \widehat{\Theta}_{\mathcal{G}_k}^{(t+1)} = \operatorname{argmin} \left\{ & -N_k^{(t)} \left[\log \det(\Theta_{\mathcal{G}_k}) - \text{tr}(S_k^{(t)} \Theta_{\mathcal{G}_k}) \right] \right. \\ & \left. + \lambda_k^{[1]} \|\Theta_{\mathcal{G}_k}\|_1 + \lambda_k^{[2]} \left(\|\Theta_{\mathcal{G}_k}^{LL} - \Theta_{\mathcal{G}_k}^{RR}\|_1 + \|\Theta_{\mathcal{G}_k}^{LR} - \Theta_{\mathcal{G}_k}^{RL}\|_1 \right) \right\}. \end{aligned} \quad (13)$$

252 We refer the readers to [Ranciati et al. \(2021\)](#), [Ranciati and Roverato \(2023\)](#) for the
 253 application of ADMM to the graphical lasso for paired data. A more detailed technical
 254 computation for updating new parameter $\Theta_{\mathcal{G}_k}$ using ADMM method is provided in
 255 Section S1 of Supplementary.

256 In summary, the pseudocode of the penalized EM algorithm for a mixture of pdRCON
 257 models is given in Algorithm 1.

258 5. Application

259 The fused penalized EM algorithm for a mixture of pdRCON models is implemented by the
 260 programming language R on synthetic and real data. Parameter initialization, model selec-
 261 tion and stopping rule of the EM algorithm will be considered in a specific case. Numerical

Algorithm 1: Penalized EM for a mixture pdRCON model

Data: samples $(\mathbf{y}_1, \dots, \mathbf{y}_N)$, regularizations $(\boldsymbol{\lambda}_1, \boldsymbol{\lambda}_2)$, maximum iteration number T_{\max}
initialization $\mathbf{w}^{(current)}$, $\Theta_{\mathcal{G}}^{(current)}$, and $t \leftarrow 0$;
while (*convergence = false*) and ($t < T_{\max}$) **do**
 (E-step) evaluate $\tau_{nk}^{(current)}$ using $\mathbf{w}^{(current)}$, $\Theta_{\mathcal{G}}^{(current)}$ by equation (9);
 (M-step) update $\mathbf{w}^{(new)}$ using $\tau_{nk}^{(current)}$ by equation (11);
 update $\Theta_{\mathcal{G}}^{(new)}$ using $\tau_{nk}^{(current)}$ by ADMM method solving (13);
 check for convergence;
 if (*convergence = true*) **then**
 break and return $(\mathbf{w}^{(new)}, \Theta_{\mathcal{G}}^{(new)})$;
 else
 $t \leftarrow t + 1$;
 $\mathbf{w}^{(current)} \leftarrow \mathbf{w}^{(new)}$ and $\Theta_{\mathcal{G}}^{(current)} \leftarrow \Theta_{\mathcal{G}}^{(new)}$;
 end
end

262 performance is presented for different sparsity and symmetry of parameters, including a
263 comparison with the glasso method for graphical Gaussian mixture models.

264 5.1. Initialization, model selection and stopping rule

265 In the application, we implement the EM algorithm with initial values of \mathbf{w} by the fractions
266 of data points assigned to each class obtained by the k-means method, and the initial values
267 of the concentration matrices are therefore considered as diagonal matrices whose diagonal
268 entries are equal to the inverse of the sample variance of the data points within the sub-
269 population, i.e. $1/(\tilde{S}_k)_{pp}$ for $p \in \{1, \dots, P\}$. This is a reasonable choice, as the variables
270 are generally at different scales in many real-life applications.

271 We apply the fused lasso for 5 different logarithmically spaced values of $\boldsymbol{\lambda}_1$ and $\boldsymbol{\lambda}_2$, in
272 particular, for every $k = 1, \dots, K$, $\Lambda_k^{[1]}/5 \leq \lambda_k^{[1]} \leq \Lambda_k^{[1]}$ and $\Lambda_k^{[2]}/5 \leq \lambda_k^{[2]} \leq \Lambda_k^{[2]}$ where
273 $\Lambda_k^{[1]} = \max |(\tilde{S}_k)_{ij}|$ and $\Lambda_k^{[2]} = \max\{|(\tilde{S}_k^{LL})_{ij} - (\tilde{S}_k^{RR})_{ij}|, |(\tilde{S}_k^{LR})_{ij} - (\tilde{S}_k^{RL})_{ij}|\}$, respectively.
274 This setting is suitable for large-scale biological datasets which encourages more sparsity
275 and symmetry constraints on parameters. Furthermore, implementing the EM algorithm
276 on an exhaustive search for $(\boldsymbol{\lambda}_1, \boldsymbol{\lambda}_2)$ over K components leads to a very costly computation,
277 hence, we will first fix $\boldsymbol{\lambda}_2$ to a low value, which could be zero, and perform the dense grid
278 search for $\boldsymbol{\lambda}_1$ over K classes. After selecting the best value of $\boldsymbol{\lambda}_1$, a grid search for $\boldsymbol{\lambda}_2$ can be
279 performed to select the final pair of optimal values of $(\boldsymbol{\lambda}_1, \boldsymbol{\lambda}_2)$. As the criteria for choosing
280 the optimal value of regularization parameters, we apply an approximation of the extended
281 BIC (eBIC) criterion (Foygel and Drton (2010)), which is computed as

$$\text{eBIC}(\boldsymbol{\lambda}_1, \boldsymbol{\lambda}_2) = -\frac{2}{N} \sum_{n=1}^N \log \left\{ \sum_{k=1}^K w_k P(\mathbf{y}_n \mid \hat{\Theta}_{(\lambda_k^{[1]}, \lambda_k^{[2]})}) \right\} + d \log(N) + 4d\gamma \log(P), \quad (14)$$

282 where $\widehat{\Theta}_{(\lambda_k^{[1]}, \lambda_k^{[2]})}$ is the penalized maximum likelihood estimation, d is the number of pa-
 283 rameters of the associated model and $\gamma \in [0, 1]$. According to [Foygel and Drton \(2010\)](#), we
 284 set $\gamma = 0.5$. The optimal choice of (λ_1, λ_2) is determined by a two-step procedure: (i) we
 285 first select the optimal values of λ_1 that are $\lambda_1^* = \operatorname{argmin} \operatorname{eBIC}(\lambda_1, \lambda_2 = 0)$, and (ii) given
 286 λ_1^* , the optimal values of λ_2 are obtained by $\lambda_2^* = \operatorname{argmin} \operatorname{eBIC}(\lambda_1^*, \lambda_2)$.

287 Regarding the stopping condition of the EM algorithm, we check the convergence by
 288 the change of the current estimate of solutions using a convenient matrix norm, i.e. if the
 289 Frobenius norm $\|\Theta_{\mathcal{G}_k}^{(new)} - \Theta_{\mathcal{G}_k}^{(current)}\|_F^2$ is less than a chosen tolerance threshold for all
 290 classes, the algorithm is stopped and has converged.

291 5.2. Simulation study

292 In this section, we conduct a simulation study of the mixture of pdRCON models in $K = 2$
 293 sub-populations. We consider three scenarios, called A, B, and C, that differ in the graphs'
 294 density degree, i.e. the ratio between the edges present in a graph and the maximum
 295 number of edges. In particular, the density degrees of the two mixture components are
 296 approximately equal to $(0.6, 0.6)$ for scenario A, $(0.15, 0.15)$ for scenario B, and $(0.15, 0.6)$
 297 for scenario C. For each scenario, we generate three pdCGs with $P = 50$ vertices on different
 298 symmetry densities between two components based on the edges present. For every pdCG
 299 \mathcal{G} , a concentration matrix $\Theta_{\mathcal{G}}$ was randomly generated such that the Gaussian distribution
 300 $\mathcal{N}(0, \Theta_{\mathcal{G}_k}^{-1})$ for each class k restricted on \mathcal{G}_k . Then 100 samples $\mathbf{y}_1, \dots, \mathbf{y}_{100}$ were simulated
 301 from the two-component multivariate normal mixture model with two different settings of
 302 the (true) mixture proportions: $\mathbf{w}^{(1)} = (0.3, 0.7)$ and $\mathbf{w}^{(2)} = (0.5, 0.5)$. To each simulated
 303 dataset, we apply the penalized EM algorithm for a mixture of pdRCON models with fused
 304 lasso proposed in (6)-(7) compared to graphical lasso introduced in (4).

305 Moreover, averaged Kullback-Leibler (KL) loss was used as a measure of model perfor-
 306 mance which is computed as

$$\frac{1}{N} \sum_{n=1}^N \log \frac{p(\mathbf{y}_n \mid \mathbf{w}^{true}, \Theta_{\mathcal{G}}^{true})}{p(\mathbf{y}_n \mid \mathbf{w}^{estimate}, \Theta_{\mathcal{G}}^{estimate})},$$

307 where $p(\cdot \mid \cdot)$ is the density function given by (5). Another measure we used here is the
 308 Frobenius norm of the difference between the true and estimated concentration matrices for
 309 each sub-population, i.e. $\|\Theta_{\mathcal{G}_k}^{true} - \Theta_{\mathcal{G}_k}^{estimate}\|_F^2$ for $k \in \{1, \dots, K\}$.

310 The quantile values of these measurements over 100 replicates are presented in Figures
 311 1-3 for the first case of mixture proportion $\mathbf{w}^{(1)} = (0.3, 0.7)$ and in Section S2 of Supple-
 312 mentary material for the second case of $\mathbf{w}^{(2)} = (0.5, 0.5)$. The recorded results of using
 313 both KL (Figure 1) and Frobenius measure (Figure 2 and 3) reveal that the fused graphical
 314 lasso for paired data we have proposed performs significantly better than the graphical lasso
 315 approach, observing that the median values for both measures from the graphical lasso are
 316 greater than the interquartile range of the fused lasso method.

317 5.3. Application to transcriptomic data

318 We consider a transcriptomic dataset originally published in [Wang et al. \(2020\)](#). Briefly,
 319 the study focused on the marine-freshwater divergence in nine-spined sticklebacks, where

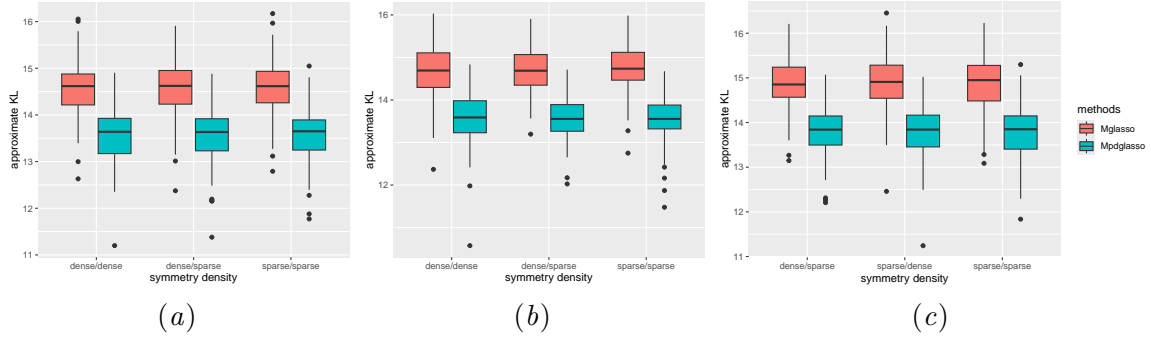


Figure 1: The quantile values of averaged Kullback-Leibler losses obtained from 100 replications of the graphical lasso method and fused lasso for the two-components pdRCON models with the mixture proportion $\mathbf{w} = (0.3, 0.7)$. Subfigures (a), (b), and (c) show the results recorded for scenario A, scenario B, and scenario C, respectively, of the generated concentrations.

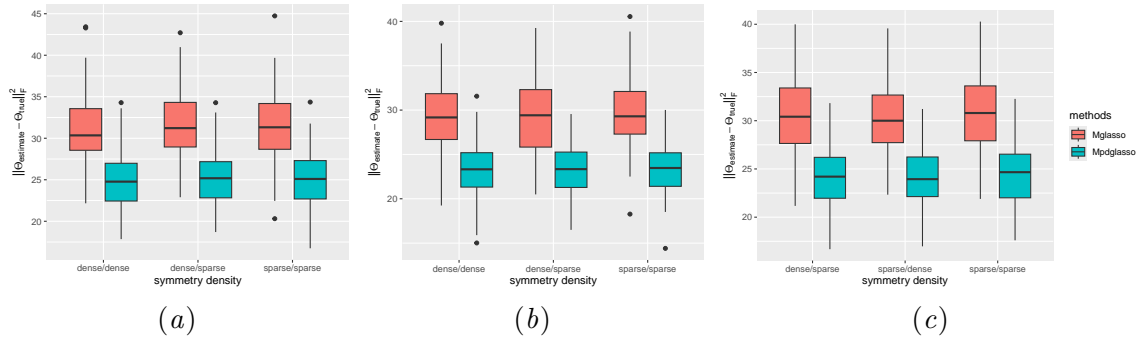


Figure 2: The quantile values of Frobenius norm values of the difference between the true and estimated concentration matrices for sub-population $k = 1$. Subfigures (a), (b), and (c) show the results recorded for scenario A, scenario B, and scenario C, respectively, of the generated concentrations of two-component pdRCON models with the mixture proportion $\mathbf{w} = (0.3, 0.7)$.

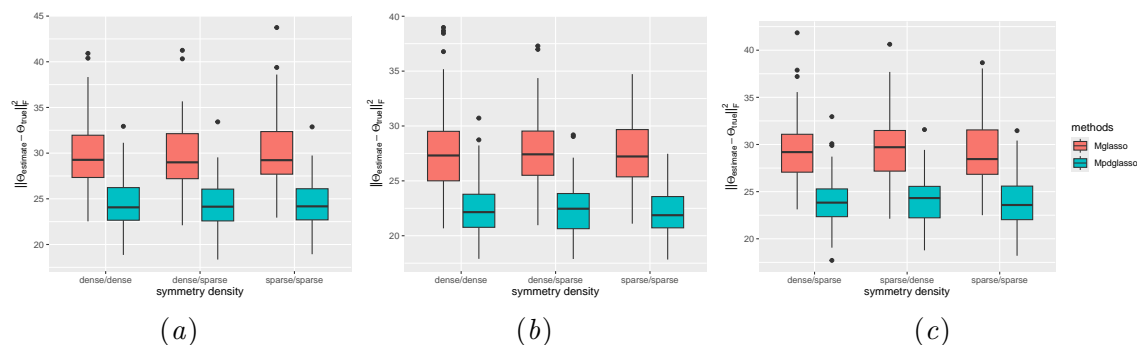


Figure 3: The quantile values of Frobenius norm values of the difference between the true and estimated concentration matrices for sub-population $k = 2$. Subfigures (a), (b), and (c) show the results recorded for scenario A, scenario B, and scenario C, respectively, of the generated concentrations of two-component pdRCON models with the mixture proportion $\mathbf{w} = (0.3, 0.7)$.

320 RNA-seq data were collected from 24 fish representing two marine and four freshwater
 321 populations in Finland and Sweden. The two groups of variables correspond to brain tissue
 322 and liver tissue, with each gene in brain tissue paired with its homologous gene in liver
 323 tissue. After filtering out genes with low variance and outliers, we selected expression data
 324 of 214 genes, comprising 107 genes from the brain and their 107 homologous genes from
 325 the liver, which were identified as top differential expressed genes in Wang et al. (2020),
 326 as a basis to estimate the gene network. We choose $K = 2$ representing the two ecological
 327 populations, i.e. marine and freshwater. In this application, we apply a mixture of pdRCON
 328 models with the following aims: (1) to evaluate whether the mixture of pdRCON models
 329 can accurately classify data points into marine and freshwater groups, and (2) to learn
 330 graphical networks that reveal distinct topological structures between the subpopulations,
 331 (3) to explore the similarity between variables in the two groups corresponding to RNA-seq
 332 data collected from brain and liver tissues, and (4) to identify a set of genes that may play
 333 a key role within the gene network.

334 The selected model classifies 6 sticklebacks into class 1 and 18 into class 2. Notably, two
 335 individuals are misclassified based on their known habitat origin. However, a principal com-
 336 ponent (PC) analysis on the same RNA-seq data, conducted by Wang et al. (2020) revealed
 337 that some marine fish collected from the Helsinki Baltic Sea are genetically closer to the
 338 freshwater population than to the marine population, according to the first two PCs. Thus,
 339 our method performs well and aligns with existing approaches in the clustering task. Figure
 340 4 illustrates the gene co-expression networks of brain and liver tissues derived from GGMs
 341 using a fused graphical lasso. This representation effectively highlights key features of the
 342 model, such as network structures and symmetries that differ between classes and tissues.
 343 Interestingly, in both habitats, the ASPG gene emerges as a hub, connected to numerous
 344 other genes. The ASPG gene has previously been reported to be expressed in response to
 345 salinity and is implicated in salt-sensitive hypertension in three-spined sticklebacks (Wang
 346 et al. (2020); Gibbons et al. (2017)), underscoring its important role in explaining fresh-

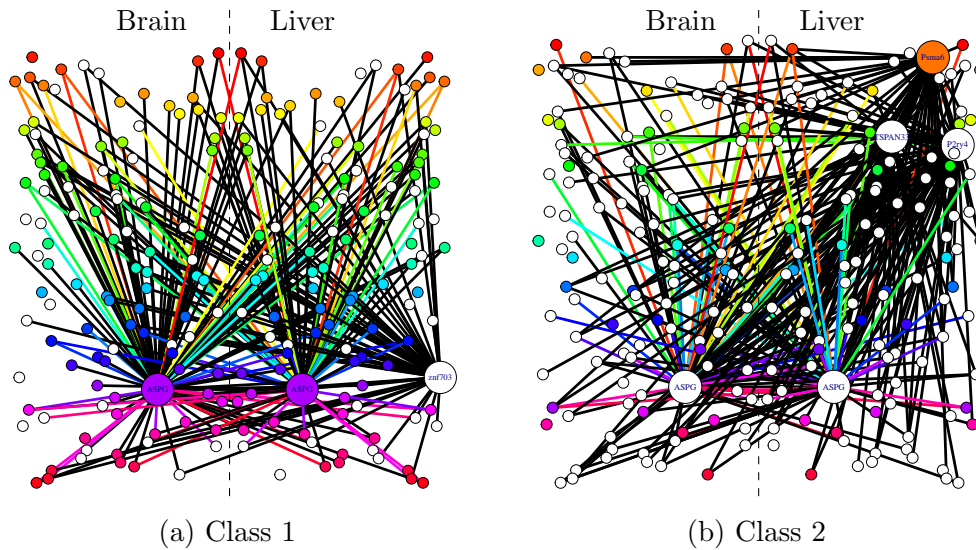


Figure 4: Colored graphical representations of gene co-expression networks highlight genes that are highly correlated with other genes in brain and liver tissues of the nine-spined stickleback collected in two habitats with (a) presenting for habitat class 1 and (b) presenting for habitat class 2.

347 water/marine divergence in sticklebacks. In addition, the network for class 2 reveals more
 348 parsimonious gene connections in the brain, while more hub genes are identified in the liver,
 349 providing an interesting direction for further biological investigation.

350 6. Concluding remarks

351 We consider high-dimensional and heterogeneous gene expression data, where observations
 352 from each sub-population originate from two dependent groups of variables across tissues,
 353 cells, or observable physical properties of an organism. We address this problem within the
 354 framework of a mixture of Gaussian graphical models, represented by colored graphs for
 355 paired data. We propose a fused graphical lasso method for maximum likelihood estimation
 356 in a mixture of GGMs for paired data, aimed at uncovering relationships between genes
 357 with expression measured under different conditions and comparing group-specific gene net-
 358 works. Our simulation studies demonstrate that the fused graphical lasso to the mixture
 359 GGMs for paired data outperforms the standard graphical lasso method in model estima-
 360 tion. Additionally, we applied our method to a high-dimensional transcriptomic dataset of
 361 nine-spined sticklebacks, collected from marine and freshwater environments across brain
 362 and liver tissues, where the number of genes greatly exceeds the number of individuals (e.g.
 363 $214 > 24$). The results align with other studies in terms of estimating gene networks, iden-
 364 tifying hub genes, classifying individuals according to common biological characteristics,
 365 and providing new insights into the differentiation of gene networks across habitats. It is
 366 also noteworthy that the mixture of pdRCON models with the fused graphical lasso can be

effectively applied in clustering scenarios with an unknown number of mixture components, which necessitates model selection based on specific criteria to determine the appropriate number of classes K . Furthermore, improving the estimation process involves the selection of an appropriate set of starting values for the parameters, as well as the development of theoretical theorems and practical techniques concerning the consistency and convergence rate of the fusion lasso penalized MLE for a mixture of pdRCON models and the overlap between mixture components in the clustering algorithm.

Acknowledgement We would like to express our gratitude for the support provided by CSIRO Agriculture and Food in undertaking this research. Our thanks also go to Dr. Jia Liu for proofreading the initial version of this manuscript and to the three anonymous reviewers for their valuable and constructive feedback.

References

- Dvir Aran, Roman Camarda, Justin Odegaard, Hyojung Paik, Boris Oskotsky, Gregor Krings, Andrei Goga, Marina Sirota, and Atul J Butte. Comprehensive analysis of normal adjacent to tumor transcriptomes. *Nature communications*, 8(1):1077, 2017.
- Mélanie Blein-Nicolas, Emilie Devijver, Mélina Gallopin, and Emeline Perthame. Non-linear network-based quantitative trait prediction from biological data. *Journal of the Royal Statistical Society Series C: Applied Statistics*, page qlae012, 2024.
- Stephen Boyd, Neal Parikh, Eric Chu, Borja Peleato, Jonathan Eckstein, et al. Distributed optimization and statistical learning via the alternating direction method of multipliers. *Foundations and Trends® in Machine learning*, 3(1):1–122, 2011.
- Edward T Bullmore and Danielle S Bassett. Brain graphs: graphical models of the human brain connectome. *Annual review of clinical psychology*, 7(1):113–140, 2011.
- Hsun-Hsien Chang and Michael McGeachie. Phenotype prediction by integrative network analysis of SNP and gene expression microarrays. In *2011 Annual International Conference of the IEEE Engineering in Medicine and Biology Society*, pages 6849–6852. IEEE, 2011.
- Patrick Danaher, Pei Wang, and Daniela M Witten. The joint graphical lasso for inverse covariance estimation across multiple classes. *Journal of the Royal Statistical Society Series B: Statistical Methodology*, 76(2):373–397, 2014.
- Arthur P Dempster. Covariance selection. *Biometrics*, pages 157–175, 1972.
- Patrik D’haeseleer, Shoudan Liang, and Roland Somogyi. Genetic network inference: from co-expression clustering to reverse engineering. *Bioinformatics*, 16(8):707–726, 2000.
- Karoline Faust. Open challenges for microbial network construction and analysis. *The ISME journal*, 15:3111—3118, 2021.
- Rina Foygel and Mathias Drton. Extended Bayesian information criteria for Gaussian graphical models. *Advances in neural information processing systems*,

- 404 23, 2010. URL [https://proceedings.neurips.cc/paper_files/paper/2010/file/](https://proceedings.neurips.cc/paper_files/paper/2010/file/072b030ba126b2f4b2374f342be9ed44-Paper.pdf)
405 [072b030ba126b2f4b2374f342be9ed44-Paper.pdf](https://proceedings.neurips.cc/paper_files/paper/2010/file/072b030ba126b2f4b2374f342be9ed44-Paper.pdf).
- 406 Jerome Friedman, Trevor Hastie, and Robert Tibshirani. Sparse inverse covariance estima-
407 tion with the graphical lasso. *Biostatistics*, 9(3):432–441, 2008.
- 408 Taylor C Gibbons, David CH Metzger, Timothy M Healy, and Patricia M Schulte. Gene
409 expression plasticity in response to salinity acclimation in threespine stickleback ecotypes
410 from different salinity habitats. *Molecular ecology*, 26(10):2711–2725, 2017.
- 411 Thomas J Hardcastle and Krystyna A Kelly. Empirical Bayesian analysis of paired high-
412 throughput sequencing data with a beta-binomial distribution. *BMC bioinformatics*, 14:
413 1–11, 2013.
- 414 Søren Højsgaard and Steffen L Lauritzen. Graphical Gaussian models with edge and vertex
415 symmetries. *Journal of the Royal Statistical Society Series B: Statistical Methodology*, 70
416 (5):1005–1027, 2008.
- 417 Zachary D Kurtz, Christian L Müller, Emily R Miraldi, Dan R Littman, Martin J Blaser,
418 and Richard A Bonneau. Sparse and compositionally robust inference of microbial eco-
419 logical networks. *PLoS computational biology*, 11(5):e1004226, 2015.
- 420 Thomas Lartigue, Stanley Durrleman, and Stéphanie Allasonnière. Mixture of conditional
421 Gaussian graphical models for unlabelled heterogeneous populations in the presence of
422 co-factors. *SN Computer Science*, 2(6):466, 2021.
- 423 Steffen L Lauritzen. *Graphical models*, volume 17. Clarendon Press, 1996.
- 424 Kevin H Lee and Lingzhou Xue. Nonparametric finite mixture of Gaussian graphical models.
425 *Technometrics*, 60(4):511–521, 2018.
- 426 Faming Liang and Bochao Jia. *Sparse Graphical Modeling for High Dimensional Data: A*
427 *Paradigm of Conditional Independence Tests*. Chapman and Hall/CRC, 2023.
- 428 Liliana López-Kleine, Luis Leal, and Camilo López. Biostatistical approaches for the re-
429 construction of gene co-expression networks based on transcriptomic data. *Briefings in*
430 *functional genomics*, 12(5):457–467, 2013.
- 431 Anani Lotsi and Ernst Wit. Sparse Gaussian graphical mixture model. *Afrika Statistika*,
432 11(2):1041–1059, 2016.
- 433 Shisong Ma, Qingqiu Gong, and Hans J Bohnert. An Arabidopsis gene network based on
434 the graphical Gaussian model. *Genome research*, 17(11):1614–1625, 2007.
- 435 Henry E Miller and Alexander JR Bishop. Correlation analyzer: functional predictions from
436 gene co-expression correlations. *BMC bioinformatics*, 22:1–19, 2021.
- 437 Saverio Ranciat and Alberto Roverato. On the application of Gaussian graphical models
438 to paired data problems. *arXiv preprint arXiv:2307.14160*, 2023.

- 439 Saverio Ranciati, Alberto Roverato, and Alessandra Luati. Fused graphical lasso for brain
440 networks with symmetries. *Journal of the Royal Statistical Society Series C: Applied*
441 *Statistics*, 70(5):1299–1322, 2021.
- 442 Xiaolan Rao and Richard A Dixon. Co-expression networks for plant biology: why and
443 how. *Acta biochimica et biophysica Sinica*, 51(10):981–988, 2019.
- 444 Alberto Roverato and Dung Ngoc Nguyen. Model inclusion lattice of coloured Gaussian
445 graphical models for paired data. In *International Conference on Probabilistic Graphical*
446 *Models*, pages 133–144. PMLR, 2022. URL [https://proceedings.mlr.press/v186/
447 roverato22a.html](https://proceedings.mlr.press/v186/roverato22a.html).
- 448 Alberto Roverato and Dung Ngoc Nguyen. Exploration of the search space of Gaussian
449 graphical models for paired data. *Journal of Machine Learning Research*, 25(92):1–41,
450 2024. URL <http://jmlr.org/papers/v25/23-0295.html>.
- 451 Rory Stark, Marta Grzelak, and James Hadfield. RNA sequencing: the teenage years.
452 *Nature Reviews Genetics*, 20(11):631–656, 2019.
- 453 Remco Ursem, Yury Tikunov, Arnaud Bovy, Ralph Van Berloo, and Fred Van Eeuwijk. A
454 correlation network approach to metabolic data analysis for tomato fruits. *Euphytica*,
455 161:181–193, 2008.
- 456 Beatriz Valcarcel, Peter Würtz, Nafisa-Katrin Seich al Basatena, Taru Tukiainen, Antti J
457 Kangas, Pasi Soininen, Marjo-Riitta Järvelin, Mika Ala-Korpela, Timothy M Ebbels, and
458 Maria de Iorio. A differential network approach to exploring differences between biological
459 states: an application to prediabetes. *PLoS One*, 6(9):e24702, 2011.
- 460 Yingnan Wang, Yongxin Zhao, Yu Wang, Zitong Li, Baocheng Guo, and Juhä Merila.
461 Population transcriptomics reveals weak parallel genetic basis in repeated marine and
462 freshwater divergence in nine-spined sticklebacks. *Molecular Ecology*, 29(9):1642–1656,
463 2020.
- 464 Ming Yuan and Yi Lin. Model selection and estimation in the Gaussian graphical model.
465 *Biometrika*, 94(1):19–35, 2007.
- 466 Zihao Zheng, Stefan Hey, Talukder Jubery, Huyu Liu, Yu Yang, Lisa Coffey, Chenyong Miao,
467 Brandi Sigmon, James C Schnable, Frank Hochholdinger, et al. Shared genetic control of
468 root system architecture between *Zea mays* and sorghum bicolor. *Plant physiology*, 182
469 (2):977–991, 2020.
- 470 Hui Zhou, Wei Pan, and Xiaotong Shen. Penalized model-based clustering with uncon-
471 strained covariance matrices. *Electronic journal of statistics*, 3:1473, 2009.